



Consistent Estimates of Tsunami Energy Show Promise for Improved Early Warning

V. TITOV,¹ Y. TONY SONG,² L. TANG,^{1,3} E. N. BERNARD,¹ Y. BAR-SEVER,² and Y. WEI^{1,3}

Abstract—Early tsunami warning critically hinges on rapid determination of the tsunami hazard potential in real-time, before waves inundate critical coastlines. Tsunami energy can quickly characterize the destructive potential of generated waves. Traditional seismic analysis is inadequate to accurately predict a tsunami’s energy. Recently, two independent approaches have been proposed to determine tsunami source energy: one inverted from the Deep-ocean Assessment and Reporting of Tsunamis (DART) data during the tsunami propagation, and the other derived from the land-based coastal global positioning system (GPS) during tsunami generation. Here, we focus on assessing these two approaches with data from the March 11, 2011 Japanese tsunami. While the GPS approach takes into consideration the dynamic earthquake process, the DART inversion approach provides the actual tsunami energy estimation of the propagating tsunami waves; both approaches lead to consistent energy scales for previously studied tsunamis. Encouraged by these promising results, we examined a real-time approach to determine tsunami source energy by combining these two methods: first, determine the tsunami source from the globally expanding GPS network immediately after an earthquake for near-field early warnings; and then to refine the tsunami energy estimate from nearby DART measurements for improving forecast accuracy and early cancelations. The combination of these two real-time networks may offer an appealing opportunity for: early determination of the tsunami threat for the purpose of saving more lives, and early cancelation of tsunami warnings to avoid unnecessary false alarms.

Key words: Tsunami energy, GPS network, DART system, early warning.

Electronic supplementary material The online version of this article (doi:10.1007/s00024-016-1312-1) contains supplementary material, which is available to authorized users.

¹ NOAA Center for Tsunami Research, Pacific Marine Environmental Laboratory, National Oceanic and Atmospheric Administration, 7600 Sand Point Way NE, Seattle, WA 98115, USA.

² Jet Propulsion Laboratory, California Institute of Technology, 4800 Oak Grove Drive, Pasadena, CA 91109, USA. E-mail: tony.song@jpl.nasa.gov

³ Joint Institute for the Study of the Atmosphere and Ocean, University of Washington, Box 355672, Seattle, WA 98105, USA.

1. Introduction

Recent tsunami tragedies have suggested clearly that a better way to detect tsunami strength is needed for early warnings. Traditional tsunami warning systems had predicted tsunami strength based on the magnitude of the generating earthquake. Unfortunately, these predictions had been largely inconsistent, resulting in inaccurate early warnings and numerous false alarms, as highlighted by Bernard and Titov (2015). Kanoglu et al. (2015—see p. 17, item 4) also emphasize the problem of tsunamigenic events with smaller earthquake magnitude, which creates another difficulty for seismic-based tsunami hazard analysis.

The two largest tsunamis of the 21st century, the 2004 Indian Ocean tsunami and the 2011 Tohoku tsunami, were initially underestimated based on early earthquake estimates. The December 2004 Sumatra–Andaman earthquake produced the most disastrous tsunami in history. However, the earthquake magnitude was initially determined as 8.0, which would indicate an insignificant ocean-wide tsunami threat. It took more than 4 h to update the seismic-based earthquake magnitude to 8.9 (ten times larger energy release), which would signal a significant tsunami threat. By that time, most of the 230,000 lives had been lost in this tsunami as the waves spread across the Indian Ocean. Although no tsunami warning system existed in the Indian Ocean in 2004 to use these tsunami threat indicators, such earthquake underestimates would be problematic for any operational tsunami warning system. Unfortunately, history repeated itself during the next mega tsunami. On March 11, 2011, a very sophisticated tsunami warning system with ample seismic data estimated the Tohoku earthquake magnitude quickly (in some cases seconds after the shaking), to be 7.9. A more

realistic estimate of the magnitude was 8.8 (differing by the same factor of 10 in the earthquake energy) obtained about 1 h later, again, after waves had already flooded Japan's coastlines. More lives could have been saved, had the size of the tsunami been determined earlier in the tsunami warning process (Ando et al. 2011).

In addition, the magnitude of the third largest earthquake of the century, the 2010 Chile event, was determined to be the final Mw 8.8 about 1 h after the shaking, again, after the tsunami waves were already inundating coastlines of Chile. Initial earthquake magnitudes determined after 7 min varied from 8.3 to 8.5, about 2–3 times smaller in magnitude estimates.

The problem is not limited to largest earthquakes only. Tsunami assessments of many smaller earthquakes based on seismic magnitude have been inconsistent; for example, the first four earthquakes in Table 1.

Each of the first four events generated tsunami warnings, and some outright local panic, but no widespread damage or tsunami-related casualties were reported. On the other hand, two relatively weak earthquakes (6 and 7 of Table 1) generated unexpectedly large tsunamis (a typical characteristic of a tsunami earthquake) that killed about 600 and 30 people, respectively.

Historically, tsunami warnings based on the earthquake magnitude have not been very successful (see for example Kanoglu et al. 2015; Titov et al. 2011). According to the 2006 US Government Accountability Office report, an unacceptable 75 % false alarm rate has prevailed in the Pacific Ocean (GAO-06-519). The currently used earthquake-magnitude-based-method for early warnings has two

shortcomings. First, early estimates of an earthquake magnitude within a few minutes after the quake are inherently inaccurate. Magnitudes of large earthquakes are often finalized hours (e.g., 2011 Tohoku tsunami, see Tang et al. 2012), days, or even months (e.g., 2004 Indian Ocean tsunami, see Stein and Okal 2005) after the shaking started. This is due to complexity of estimating full energy released by the shaking, which may not be captured well by even modern seismometers. For smaller earthquakes, lack of nearby seismic data may lead to large uncertainties in magnitude. So precise determination of the earthquake magnitude in the first few minutes is still a challenge. Secondly, even when the magnitude of an earthquake can be established quickly, this magnitude does not necessarily correlate well with the size of a resulting tsunami. Okal (2015) reached similar conclusions considering challenges of real-time and post-event tsunami hazard assessments based on seismic data. His analysis of 17 tsunami events since 2004 demonstrated mixed results of tsunami warning performance based on earthquake magnitude analysis. Specifically, 'tsunami earthquakes' were singled out as one of the main challenges for real-time warning. The 'tsunami earthquake' generates larger tsunami than the seismic source magnitude would suggest. Mild shacking of 'tsunami earthquakes' create problems for the real-time seismic magnitude assessments, as well as for the near-field response measures, since both of those depend on shaking intensities. While improvements in both areas (seismic analysis with W-phase and educating population about duration of shaking) are evident, the large uncertainties of real-time response during 'tsunami earthquakes' remain to be a major challenge.

Table 1

Examples of recent earthquakes, their magnitudes did not scale the resulting tsunamis

1	March 2005	Nias Island	M _w 8.6	Over-warning (Okal 2015)
2	June 2005	West California	M _w 7.2	Tsunami warning for a strike-slip event. No coastal impact
3	May 2006	Tonga	M _w 8.0	Tsunami warning issued, no tsunami damage (Tang 2008)
4	April 2012	Sumatra	M _w 8.6	Over-warning (Okal 2015)
5	November 2006	Kuril Islands	M _w 8.3	Under-warning (Okal 2015)
6	July 2006	West Java	M _w 7.7	Tsunami earthquake (Okal 2015). No early warning was issued out of fear of false alarms (Jouhana and Paddock 2006)
7	April 2007	Solomon	M _w 8.0	Tsunami earthquake (Satake et al. 2013)

Tsunami generation is different from the earthquake dynamics or rupture that can be measured by seismic instruments. The earthquake magnitude is proportional to the energy released by the earthquake shaking, while the tsunami energy is measured by how much the ocean water is displaced (Song et al. 2008). As a rule of thumb, the tsunami energy is only a small fraction (typically, about 0.001) of the energy released by the generating earthquake (Tang et al. 2012). Therefore, it is difficult to predict a tsunami's energy from the earthquake energy alone. Besides, measurements of earthquake shaking (seismic data) do not capture other tsunami generating processes, such as slumps.

The difficulty of establishing fast and robust measures of a tsunami's potential impact has been long recognized by tsunami research. Initially, tide gauge records and post-event surveys were the only non-earthquake measures of tsunami intensity. Several tsunami intensity and magnitude scales based on these coastal tsunami data have been proposed (e.g., Sieberg 1927; Imamura 1942; Iida 1956; Ambraseys 1962; Papadopoulos and Imamura 2001). However, none of the proposed tsunami intensity and magnitude scales based on these coastal tsunami measurements has become practical tools, or has been accepted as reliable objective assessments. Two main reasons are: (1) tsunami run-up heights are dominated by local coastal morphology, which makes it very difficult to interpret as a global measure of tsunami impact, and (2) coastal data are of limited forecast value for early local warnings. Realizing these limitations, Murdy and Loomis (1980) proposed to use the tsunami potential energy for estimating a tsunami size. They argued that an energy scale, based on moment magnitudes or deep-ocean tsunami measurements, would unambiguously provide an objective and quantitative means of expressing the tsunami threat. Unfortunately, there was no technology to measure tsunamis in the deep ocean at that time and moment magnitudes have not provided the accuracy needed for real-time warnings.

Recently, two practical approaches based on coastal GPS data (Song 2007) and deep-ocean tsunameter measurements (Tang et al. 2012) have been proposed for determining tsunami energy. Method 1 uses an innovative approach to determine

tsunami energy and scales directly from coastal GPS network for early warnings (see Figs. 1a, 2b). The GPS approach focuses on estimating tsunami source (potential and kinetic) energy directly from coastal GPS-measured seafloor motions (Song 2007; Song et al. 2012; Xu and Song 2013). Particularly, Song (2007) argued that GPS-derived seafloor motions are the earliest indicators of the tsunami potential, since their estimation directly relates to the mechanism that generates tsunamis. The drawback of this approach is that the predicted tsunami size cannot be confirmed by GPS measurements alone and, therefore, may carry significant uncertainties. Method 2 uses NOAA's operational tsunami propagation model to estimate tsunami energy during the tsunami propagation by assimilating real-time deep-ocean tsunami measurements from Deep-ocean Assessment and Reporting of Tsunami (DART or tsunameter) stations (Fig. 1b). Tang et al. (2012) showed that the DART-derived energy estimate was available within 56 min of the time of generation during the 2011 Japanese tsunami. During the real-time assessment of the September 16, 2015 Chile tsunami, the earliest estimate of tsunami energy, which differs only by 2–13 % to the final estimates, was obtained with the first quarter-wave of DART recording 40 min after the earthquake (Tang et al. 2015). The main drawback to this method is that a DART station must first measure the tsunami to estimate the energy. Therefore, the proximity of the nearest DART station to the earthquake determines how soon the estimate is available.

Both methods are real-time estimation and can become operational for early warnings. They are independent of each other in methodology and based on different observational systems: one inverted from the real-time deep-ocean DART data during a tsunami propagation, and the other derived from the land-based GPS measurements during tsunami generation. Therefore, these methods can potentially compliment each other to provide faster and more accurate measure of tsunami energy, if used together. Two important issues will be discussed in this paper: (1) do both methods estimate similar energy for a given tsunami, and (2), can the methods be used in combination to improve early warnings? In the next section, the two methods will be compared for

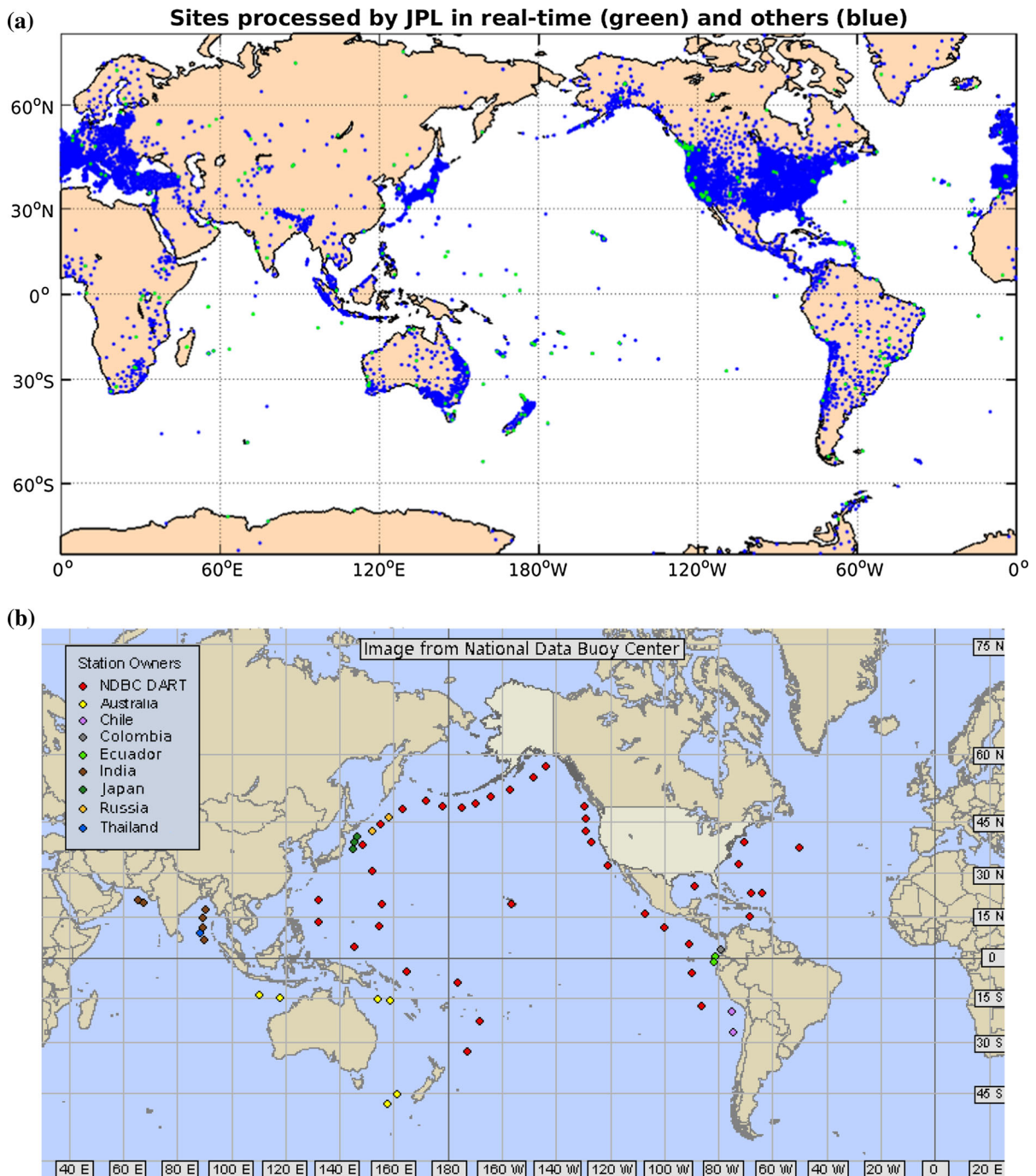


Figure 1

The land-based GPS and ocean-based DART networks. **a** NASA global differential GPS (GDGPS) tracking sites (*green dots*) and other continuously processed GPS sites (*blue dots*), which become increasingly available in real-time. **b** The global DART network system operating by nine countries

estimating the energy of the 2011 Japan tsunami. In Sect. 2, discussion focuses on the practical issues of tsunami energy determination. The final section

offers a summary and discussions. Technical details are provided in Appendices 1 and 2 or through supplemental online materials.

2. Tsunami Energy Determinations

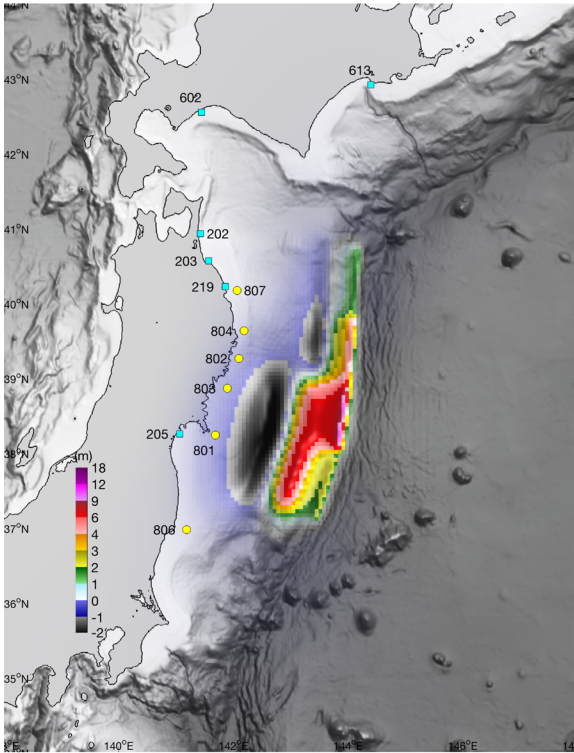
The 2011 Japan tsunami provided sufficient GPS data and DART measurements to assess GPS- and DART-derived energy estimates. To evaluate consistency of energy estimates of both methods and avoid additional uncertainty of different tsunami propagation models, we have simulated corresponding tsunamis with the same MOST tsunami model (Titov and Synolakis 1995, 1998; Titov and Gonzalez 1997). Figure 2a, b shows the initial conditions for the DART- and GPS-derived sources, respectively. As shown in Fig. 2a, the maximum initial sea-surface elevation of the DART source is 10.3 m. This tsunami initial condition is based on the pre-determined earthquake source divided into 100 km by 50 km cells along the fault (Tang et al. 2012). The seafloor deformation is considered to be identical to the sea-surface elevation. Differently in Fig. 2b, the GPS source has both initial seafloor deformation and velocity, with a maximum initial seafloor deformation of 6.8 m and horizontal velocity of 0.52 m/s, respectively. The horizontal velocities are derived from GPS displacements (Song 2007; Song et al. 2012) and indicated by blue arrows in Fig. 2b. The vertical deformation of seafloor is consistent with the frontal wedge uplift of 5 m, measured by Ito et al. (2011) near the source region, plus a contribution of the slope displacement (Tanioka and Satake 1996). Note that the GPS source changes during the earthquake rupture process over the first few minutes of tsunami generation. However, for simplicity, both sources (or initial conditions) have been applied to the MOST model instantaneously. As a result, the initial GPS source energy computed with this MOST simulation is slightly different from the estimates published by Song et al. (2012). Figure 2c, d shows the computed maximum tsunami amplitude in the near-field from the two sources. The figures demonstrate that the differences in maximum amplitude patterns are limited mostly to the near-source area. For example, areas with greater than 2 m difference in maximum amplitude are between 37.6 and 38.9°N (140 km wide). For differences greater than 5 m, those areas are between 38.12 and 38.49°N (42 km wide). Despite these differences, impacts of modeled tsunamis from the two sources on the Japanese

coastline and their propagation patterns in the far field are fairly similar, with only few locations of significantly different amplitudes. As will be discussed later, comparisons with DART and coastal tide gauge data in both near and far fields also show that the source differences have little effect on the maximum wave amplitude at those locations.

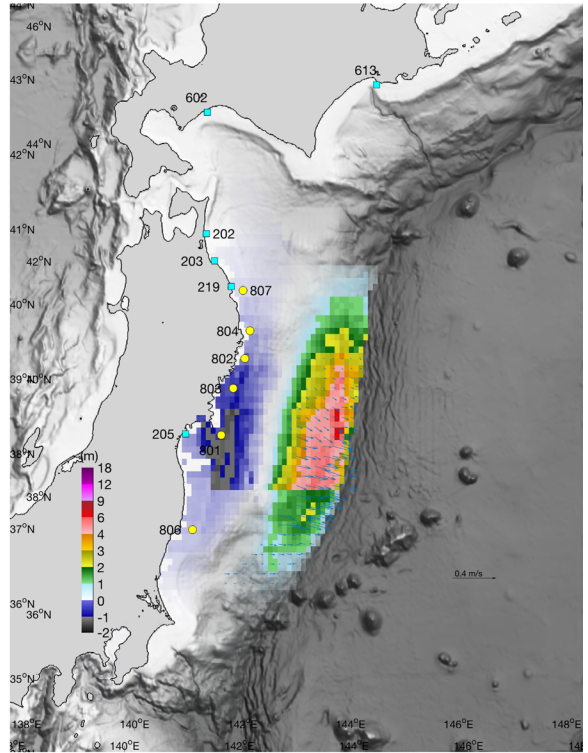
The comparisons of the two simulated tsunamis at both near-field stations (Fig. 3) and the 30 DART stations (Fig. 1b) demonstrate the similarities of the tsunami propagation dynamics for both sources. In Fig. 4, we compare the two simulations with time series at deep-ocean DART stations. It can be seen that the waves in the far field are not very sensitive to details of the initial ocean surface deformation, as long as the total energy and the general source location are correctly determined. This further confirms that tsunami energy is a critical source parameter. Smaller-scale details, such as the exact ratio of kinetic energy (KE) and potential energy (PE) at the initial stage, are of second order importance for the characterization of tsunami propagation in the far field. As pointed out in Tang et al. (2012), the tsunami propagation is strongly affected by the seafloor topographic features. Degueldre et al. (2016) also point out importance of topographic features. The comparisons at 33 far-field coastal tide stations (supporting online materials Figures S1, S2) also reinforce the above conclusions.

Figure 5 shows the model-data comparisons at 12 near-field NOWPHAS GPS buoys and wave gages along Japan coasts (locations can be found in Fig. 3). In general, the two sources produce similar wave amplitudes except at the two stations 801 (5) and 803 (4), where the GPS source significantly overestimated the first wave. Stations 801 and 803 are closest to the earthquake epicenter. The measured maximum (also the first) wave is 5.8 and 5.7 m at the two stations, while the GPS source shows 17.7 and 9.3 m, respectively (with an error of 200 and 68 %, respectively). The DART source shows 7.7 and 5.3 m at the two stations (with an error of 32 and -7 %, respectively). Some of the differences may be caused by the seafloor subsidence due to the earthquake. The differences demonstrate sensitivity of the GPS inversions to small-scale details of the tsunami source that manifest themselves at locations in the

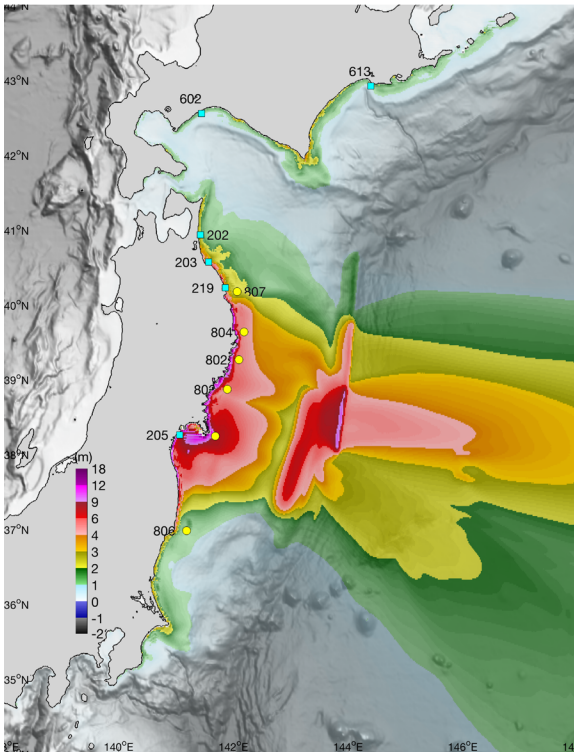
(a)



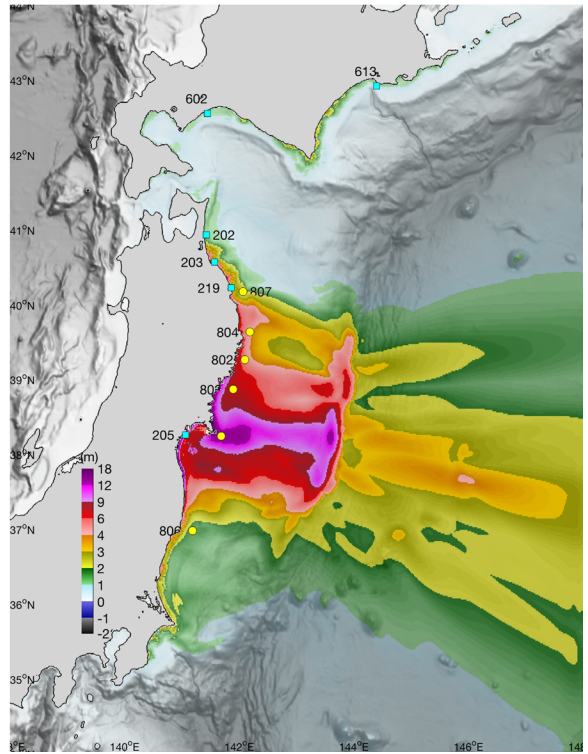
(b)



(c)



(d)



◀Figure 2

Initial bottom deformations of the **a** DART- and **b** GPS-derived tsunami sources for the 2011 Japan tsunami. *Arrows in c* are the initial velocity of the GPS source. Maximum computed offshore amplitudes were plotted in **c** for the DART source and **d** for the GPS source

immediate proximity to the source. In addition, the complex bathymetry around station 801 may also contribute to the larger error. Another notable difference is the sign of the first wave amplitude at some coastal locations. DART-derived model results show larger negative amplitude of the leading wave when compared with GPS-derived solution and with observations.

Nevertheless, the later waves modeled by both sources are in good agreement with the observations for both amplitude and wave period. This is consistent with previous theoretical and laboratory conclusions that asymptotic (beyond 20 times of the water depth or about 100 km from the source for an average ocean depth of 5 km) wave trains are insensitive to source details (Fig. 5 of Hammack and Segur 1974). More recent modeling studies of tsunami propagation (Titov et al. 2005; Satake et al. 2013; Okal and Synolakis 2016) emphasized even stronger influence of tsunami propagation dynamics on waves signal at coastlines. The results indicate that it is the local bathymetry, coastline shape and tsunami dispersive qualities rather than the details of the remote source that determine the later waves in the mid- or far-field. This conclusion suggests that it may be difficult to determine details of forcing mechanism of tsunami (or the tsunami source) just from mid- and far-field observations (Song et al. 2005). It is still challenging to obtain enough near-source observations, particularly in real time, to validate the two competing tsunami forcing mechanisms (Song and Han 2011). Fortunately, our present study demonstrates a practical method to focus on their consistent energy scale rather than the source details for early tsunami warnings.

Figure 6a, b shows the inundation comparisons at Sendai, Japan and Kahului, Hawaii, respectively. Similar high-resolution tsunami flooding estimates are slowly becoming standard tsunami warning products for many coastlines thanks to the

advancement in the internet and advancement in computer modeling (Titov et al. 2011). The results illustrate the consistency of the tsunami impact to the coastal areas for the two sources. Sendai was one of the most severely inundated areas in Japan during the 2011 tsunami. Both sources accurately reproduced the inundation limits (Fig. 6a). There are several reasons: (1) the tsunami travel time to Sendai is about 1 h after the earthquake origin time (Tang et al. 2012), while it takes no more than half an hour for the conversion of total tsunami energy (E_T) to wave energy for both DART and GPS sources. In other words, Sendai is located outside the area that is sensitive to the source details. (2) The dominant influence of topography (in addition to bathymetry) on inundation further diminishes the influence of source differences. (3) As pointed out by the near-field modeling study in Wei et al. (2013), later waves arrived more than 2 h after the tsunami generation caused the greatest penetration of inundation at some locations in Sendai. We have seen that the later waves from the two sources are quite similar (Figs. 3, 4). At Kahului, Hawaii, detailed inundation observations are not available. However, examination of damage survey video taken from a helicopter at daybreak on March 12, 2011 (<https://www.youtube.com/watch?v=qRZvK7FG020>) revealed good qualitative agreement with the forecasted flooding. In coastal areas with relatively steep slope, the two sources produce nearly identical inundation. In areas with flat slope, such as the flat areas and the lagoon to the southeast of Kahului Harbor, the DART source produced a slightly greater area of inundation. In summary, similar incident waves produce similar inundation pattern at the given location.

Energy estimates may be applicable to all kinds of tsunamis caused by landslides, volcanoes, asteroid impacts and other generation mechanisms, because energy is a common quantity. Regardless of the forcing mechanisms, the ocean must receive enough energy to generate tsunamis. Detecting the source energy transferred to the ocean is the key to the determination of tsunami hazard potential (Morgan 2011). Formulations for calculating the source energy have been detailed in Song (2007), Song et al. (2008) and Tang et al. (2012) and are also described briefly in the Appendices 1 and 2.

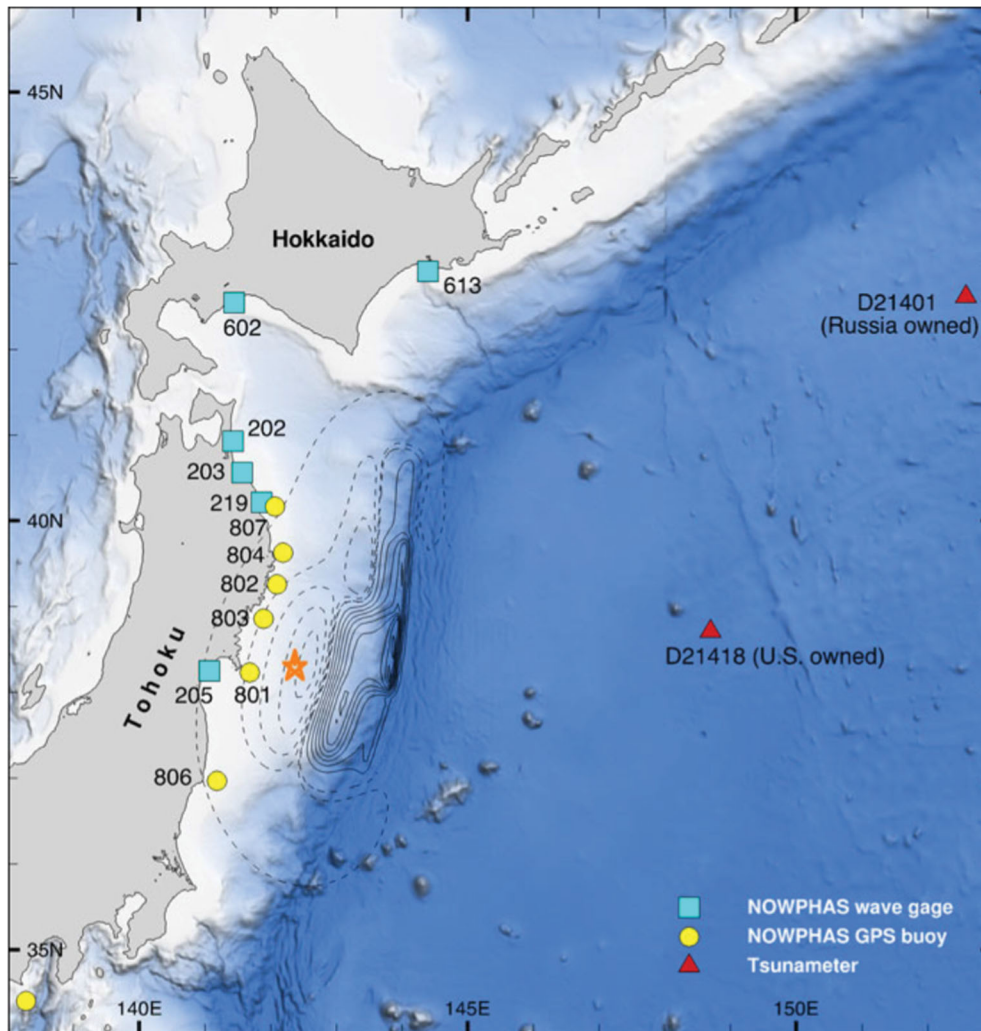


Figure 3
Locations of the NOWPHAS wave gages and GPS buoys in near-field

Using the formulations, we have compared energy of previously studied tsunamis listed in Table 2. We have included earthquakes with magnitude greater than 8 that have been analyzed using both considered methodologies. Figure 7 illustrates the two tsunami energy estimates for each event, with the events ordered by earthquake magnitude. The figure illustrates once again that the earthquake magnitude is not a good predictor of the tsunami energy. For example, events from Mw 8.0 through Mw 8.7 show tsunami energy comparable within the uncertainty of estimates, while the earthquake energies differ by one order of magnitude. The figure also shows that the

two approaches are consistent in estimating tsunami energy; however, the differences in some cases are substantial. The differences appear to be related to the quality of the data used for the estimates. Larger discrepancies are for those earthquakes where GPS or DART data were insufficient. Among all these cases, the 2011 Japanese tsunami gives the closest comparison because this event provides high-quality land GPS and DART data for those calculations. Therefore, we consider this study as showing promising consistency for real-time tsunami energy estimation. If these two approaches are used in tandem, they may provide consistent assessment of tsunami hazard,

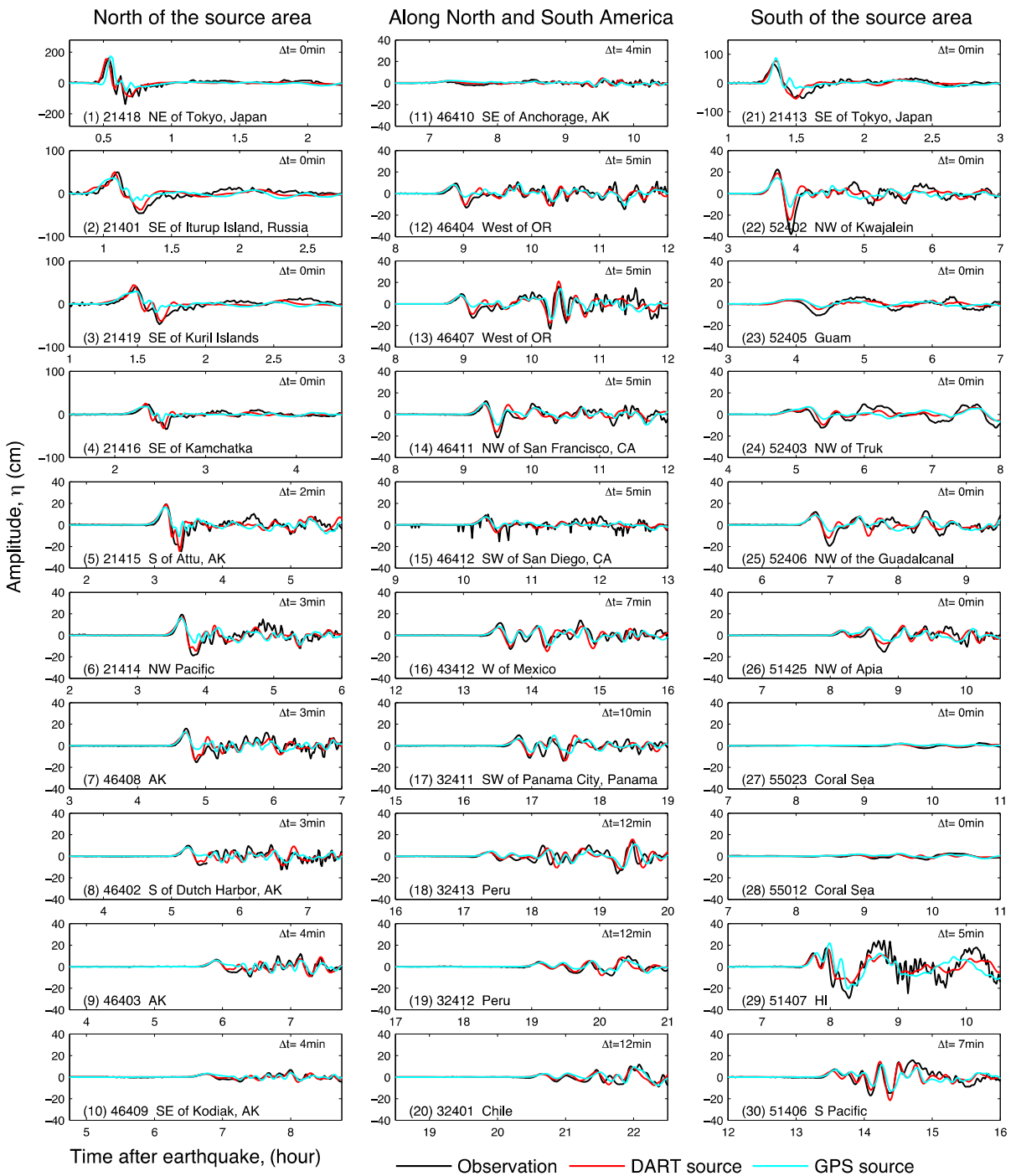


Figure 4

Observed and modeled tsunami amplitude time series at deep-ocean DART stations (Figs. 1b, 3) for the 2011 Japan tsunami. Red and cyan lines are computed from the DART- and GPS-derived sources, respectively

earlier and more accurately than other existing methods. An early test of these two approaches (e.g., Gusman et al. 2012; Wei et al. 2014) for the 2011

Japanese tsunami showed that the GPS and DART data could be used jointly for estimation of the tsunami source.

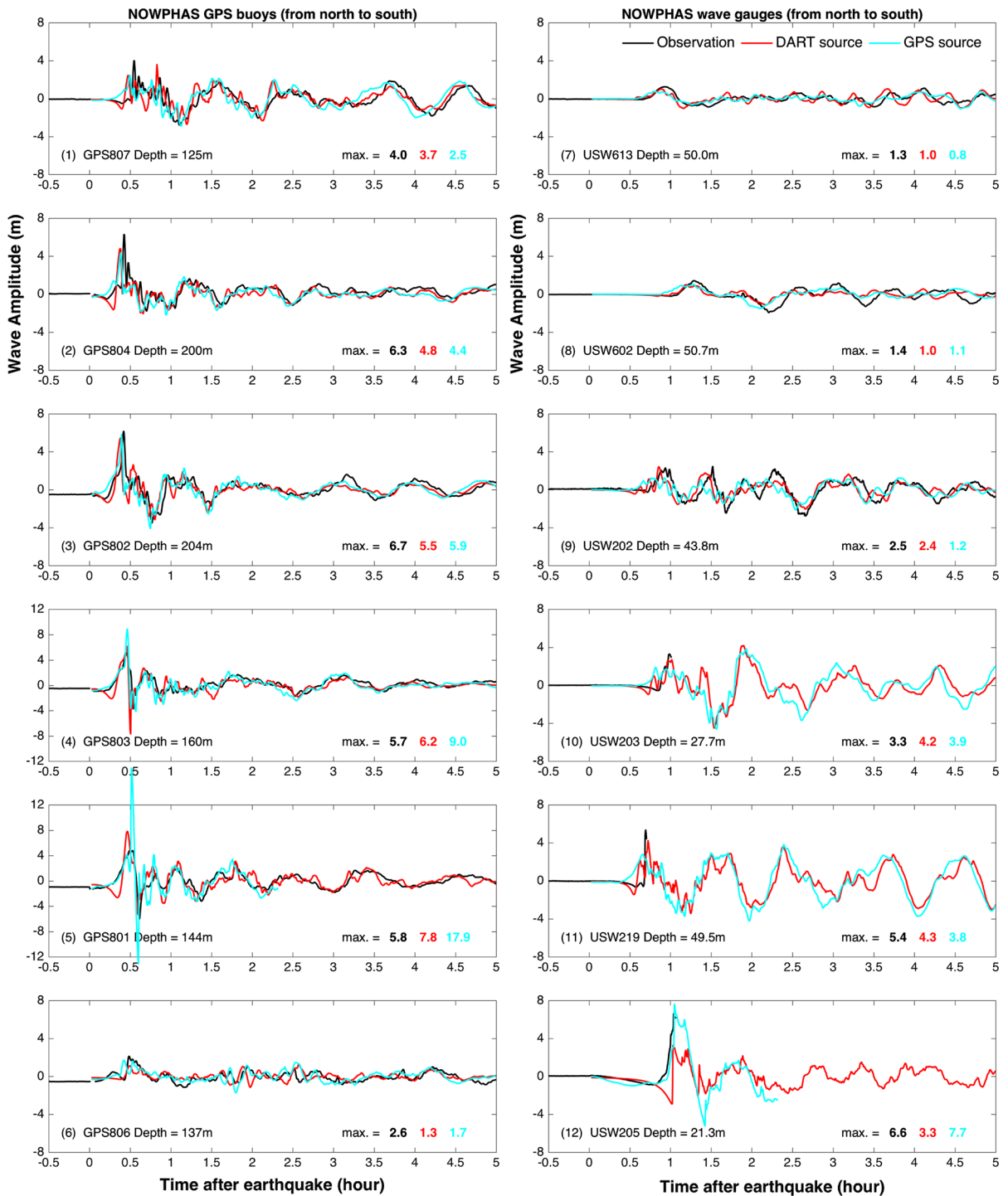


Figure 5

Observed and modeled tsunami amplitude time series at nearshore NOWPHAS GPS buoys and wave gages (Fig. 3). Red and cyan lines are computed from the DART- and GPS-derived sources, respectively. The maximum crests of the observation, DART and GPS sources are listed after “max=” in each figure

3. Summary and Conclusions

In this study, we have investigated the consistencies of the two independent approaches for tsunami energy determinations: one from the land-based GPS measurements and the other inverted from the ocean-based DART data. Because of the high-quality GPS and DART data, the 2011 Japan tsunami has been used as the benchmark for the comparison. The GPS-derived source was assimilated into NOAA's operational tsunami forecast system to evaluate its potential application for tsunami forecasting. The 2011 Japan tsunami provides the best available and comprehensive tsunami and GPS data comparison to date.

While the GPS-derived source takes into consideration the dynamic earthquake process, the DART-inverted source assumes instantaneous ocean surface displacements and zero initial velocity. Nevertheless, the tsunami source energy is similar for both approaches. They provide consistent results for coastal water level stations, for DART locations, and for flooding estimates in the near and far fields. The study shows the ability of GPS-derived source to properly estimate the tsunami wave energy early in the tsunami generation stage. The results also indicate that GPS-derived source details may lead to inconsistencies with tsunami measurements in some areas, especially in the near-field. Therefore, it is important to use the DART-derived source based on direct tsunami measurements, to further quantify and improve accuracy of the propagating wave energy, since it is the tsunami wave energy at the propagation stage that determines coastal impacts.

Both GPS- and DART-derived tsunami energy estimates can be achieved in real time and can be used for the real-time tsunami threat assessment as long as sufficient data from nearby GPS and DART stations are available. As shown in Fig. 1, there are several locations in the world today where the position of coastal GPS stations and DART stations can provide tsunami energy estimates within 20 min. Clearly, more GPS and DART stations will be required to expand the locations where quick energy estimates can be achieved to provide useful real-time assessment for coastal communities. By combining these two real-time networks and the two source

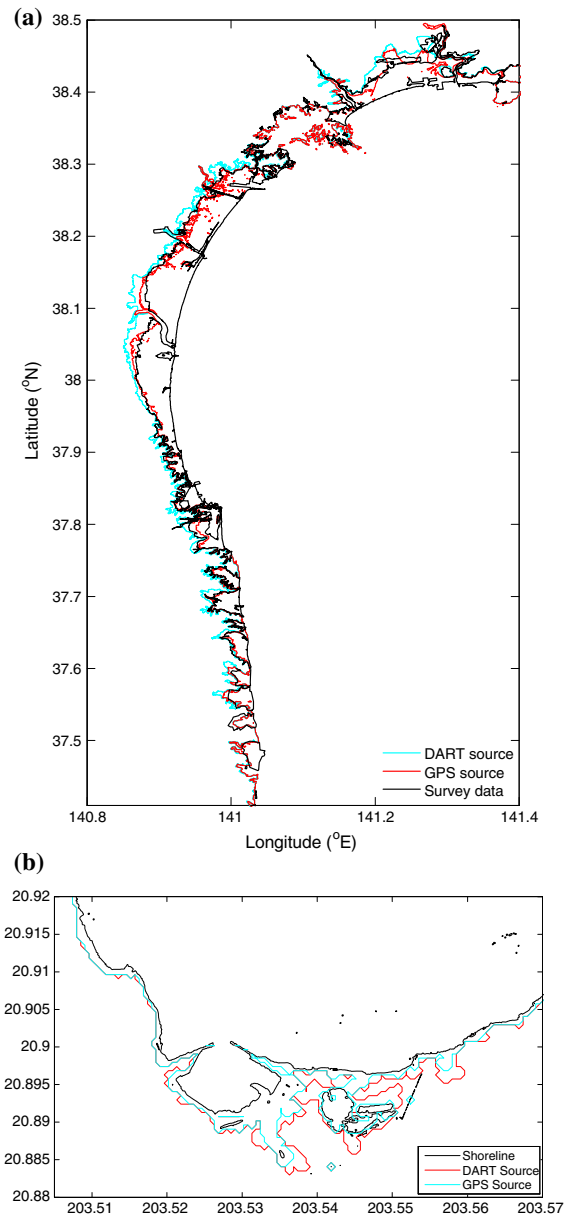


Figure 6

Inundation comparisons at **a** Sendai and **b** Kahului for the 2011 Japan tsunami. Red and cyan lines are inundation limits computed from the DART- and GPS-derived sources, respectively. The black lines in **a** are survey data

inversion methods demonstrated here, we can potentially improve tsunami early warnings efficiency and forecast accuracy through more rapid and accurate tsunami energy estimates. One shortcoming of the DART inversion approach is the time required for a tsunami traveling to the nearest DART station,

Table 2
Tsunami-source energy based on GPS and DART measurements

Earthquake and magnitude		Tsunami energy (J) (E_T)	
		GPS	DART
1964 Alaska	9.2	8.2×10^{15a}	4.2×10^{15a}
2004 Sumatra	9.1	6.0×10^{15}	1.6×10^{16a}
2005 Nias Island	8.7	2.8×10^{14}	
2006 Tonga	8.0		7.3×10^{13}
2006 Kuril	8.3	1.2×10^{14a}	6.2×10^{13}
2007 Kuril	8.1		2.2×10^{13}
2009 Samoa	8.1	3.5×10^{14}	1.2×10^{14}
2010 Chile	8.8	6.5×10^{14}	1.6×10^{15}
2011 Japan	9.0	3.2×10^{15}	3.0×10^{15}

^a Using seismic or tidal data (GPS or DART data not available). See details in Song (2007) and Tang et al. (2012)

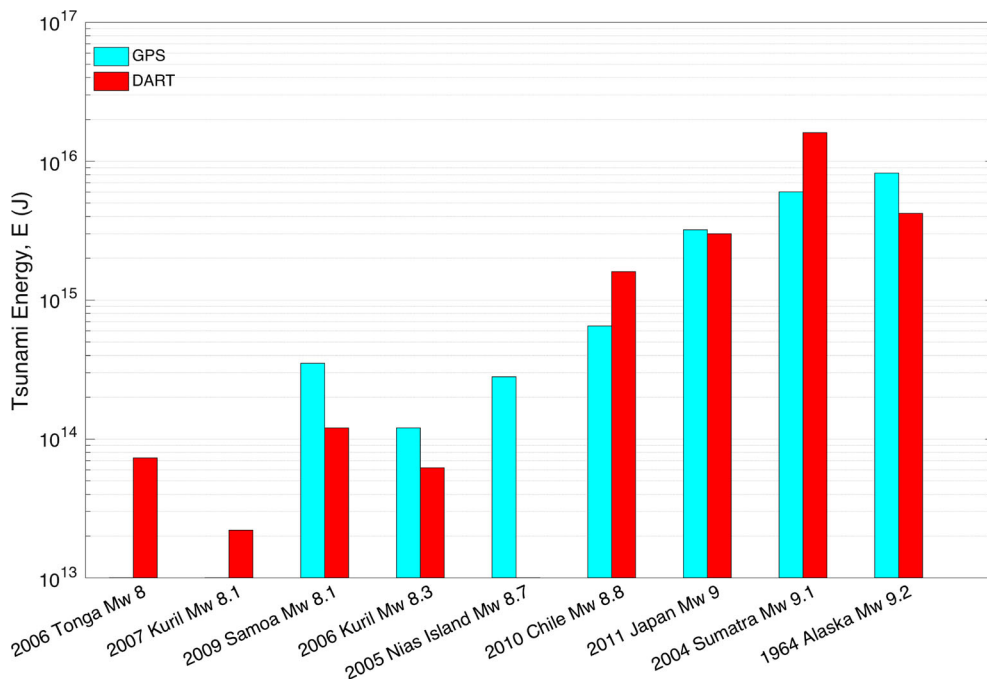


Figure 7

Tsunami-source energy based on GPS and DART measurements for past events. Seismic or tidal data were used when GPS or DART unavailable (see Table 2 for details)

which may take hours for some tsunami sources with existing DART array (Bernard et al. 2014). New DART 4G could provide faster detection but that system is still being tested and is not operational yet. The shortcoming of the GPS-based tsunami

assessment is the fact that multiple GPS stations should be in the immediate proximity of a tsunami source where substantial crustal deformations occur. If GPS-derived tsunami sources are computed within few minutes (in places where sufficient GPS stations

exist) and complement DART inversions, the combination of these two methods could provide the following advantages for future tsunami forecast:

1. Improve near-field early warnings and save lives. About 99 % of tsunami victims are local. The GPS-based inversion can directly estimate seafloor displacements, aiming to predict tsunami energy as quickly as 5 min following the earthquake and enabling an early alert to local communities.
2. Reduce false alarms and increase reliability. To avoid possible bias from the land-based GPS measurements of the earthquake, the DART measurements can be used to derive tsunami estimates based on direct tsunami observations to verify and improve the GPS-aided initial energy estimates and forecast.

The combination of the two real-time networks for tsunami early warnings is different from the currently used earthquake-magnitude-based-method using seismic data, by tsunami warning centers in Japan, Europe and Indonesia. Our research shows potential of using both data and data-derived tsunami energy for the early tsunami warning applications. The combination of the GPS data with the existing DART network can provide an effective and inexpensive solution for early detection of tsunami hazards to save lives with early forecast and warning and for early cancellation of tsunami warnings to avoid unnecessary false alarms.

Acknowledgments

This research is partially funded by the NOAA Center for Tsunami Research, PMEL contribution 4405, and by the Joint Institute for the Study of the Atmosphere and Ocean (JISAO) under NOAA Cooperative Agreement NA10OAR4320148 (2010–2015) and NA15OAR4320063 (2015–2020), Contribution No. 2497. Part of the research carried out by Y. T. Song and Y. Bar-Sever here was conducted at the Jet Propulsion Laboratory, California Institute of Technology, under contract “GPS-Aided and DART-Ensured Real-time (GADER) Tsunami Early Detection System” with the National Aeronautics and Space Administration (NASA).

Appendix 1: GPS Method

The Global Navigation Satellite System (GNSS) (including American GPS, Russian GLONASS, Chinese Beidou, European Galileo, Japanese QZSS, and Indian IRNSS) will soon emerge as a practical technology for monitoring, forecasting and rescue management and future planning. By 2020, there will be over 160 GNSS satellites broadcasting over 400 signals across the L-band, nearly double the number today at any location. Currently, there are increasing numbers of dense GNSS networks with hundreds of stations that can and do provide real-time data in coastal regions that have a history of great tsunami-genic earthquakes, including the Cascadia subduction zone, the Japanese archipelago, and the Southern American trench. This represents an untapped new valuable data source for tsunami and earthquake early warning.

NASA has funded the early development of a prototype real-time GPS-based rapid earthquake and tsunami characterization system (<http://www.nasa.gov/topics/earth/features/tsunami-20080117.html>). Real-time GPS data, in various forms and processing stages, were primarily from the NASA Global Differential GPS System (GDPS—<http://www.gdgps.net>). With 150+ real-time GPS receivers, it is the world’s largest globally distributed, centrally managed real-time GPS network. The GDGPS system is a high accuracy GPS augmentation system, developed by JPL, to support the real-time positioning, timing, and orbit determination requirements of NASA science missions. Its real-time products are also used for GPS situational assessment, natural hazard monitoring, emergency geolocation, and other civil and defense applications.

The utility of GPS data for earthquake magnitude determination and for tsunami monitoring was demonstrated by Blewitt et al. (2006) who showed how the correct magnitude of the 2004 Sumatra earthquake could have been determined in near real time by complementing the seismic data with measurements from relatively few GPS tracking sites. Song (2007) demonstrated that coastal GPS stations are able to detect continental slope displacements of faulting due to large earthquakes and the GPS-detected displacements are able to estimate the

disturbed oceanic energy and tsunami scales within a few minutes after the quake. This innovative method has been successfully tested in a NASA pilot program—the GPS-aided Real-Time Earthquake and Tsunami (GREAT) Alert System, during the events of the 2010 Chilean M 8.8 earthquake and associated tsunami (NASA release 2010: http://www.nasa.gov/topics/earth/features/tsunami_prediction.html; Nar-anjo 2013). The basic steps are the following: (1) locate an earthquake epicenter from seismometers (a few minutes after an initial earthquake); (2) collect near-field GPS-derived land velocities and infer the seafloor motions (a few more minutes of latency are possible); and (3) calculate the tsunami energy based on the GPS-predicted seafloor motions and local topography. For locations with real-time GPS coastal station and an earthquake model that includes local topography, the time to estimate the tsunami energy could be as little as 5 min after earthquake origin time. This approach was further tested after the 2011 Japan tsunami (Song et al. 2012; Xu and Song 2013).

For completeness, here we briefly describe the GPS approach. Notice that GPS stations only measure near-source ground motions of faulting, not the undersea ground motions that generate tsunamis. Therefore, the seafloor displacements due to the earthquake have to be derived from near-source GPS measurements. Although sophisticated GPS-inversion models have been explored using the shear and tensile fault theory in a half-space (Okada 1985), for tsunami prediction, we only need the seafloor (surface) displacements. Because great earthquakes cause large-scale ground motions, the coastal GPS-measured displacements are part of the major motions at the fault. Therefore, the seafloor displacements can be projected or extrapolated from the near-source GPS measurements. For tsunami early warnings, time is of the essence. To get the tsunami source from the real-time GPS measurements without delay, Song (2007) formulated an empirical profile extrapolation to project the seafloor displacements.

The formulation is as follows. Let $(\Delta E_j, \Delta N_j)$ be the near-field GPS offsets (horizontal displacements) in the eastward and northward direction, respectively, where Δ represents a small increment. The subscript j labels the GPS stations alongshore (parallel to the

fault line), but only for those closer stations. For each j station, a cross-shelf section through the station, usually perpendicular to the fault, is identified. The seafloor displacements along the cross-shelf section are modeled to follow an empirical profile until the frontal edge of the fault (the trench):

$$\Delta E(r) = \Delta E_j \exp(r_j^2 - r^2) + \Delta e_{j2} \quad (1)$$

$$\Delta N(r) = \Delta N_j \exp(r_j^2 - r^2) + \Delta n_{j2} \quad (2)$$

$$\Delta U(r) = \alpha \sqrt{\Delta E(0)^2 + \Delta N(0)^2} \times \left\{ \exp(-ar^2) - \sqrt{\frac{\pi}{4a}} \exp(-r) \right\} \quad (3)$$

Here, $r = d/W$ is the normalized distance such that $r = 0$ on the fault line and $r = r_j$ at the j -th GPS station and, d is the physical distance from the fault line perpendicularly, and W is the mean distance of the GPS stations from the fault. An empirical value of $W = 320$ km is used for the 2004 Sumatra and 1964 Alaska earthquakes and 250 km for the 2011 Tohoku earthquake. If more GPS stations are available (besides the j labeled stations), a least-square fitting between the model results and the data is used for $(\Delta e_{j2}, \Delta n_{j2})$ to correct the projection, where the $j2$ represents the extra GPS stations. The vertical uplift/subsidence is determined from the horizontal displacements by conserving mass such that the uplift volume equals the subsidence volume, in which the non-dimensional constant $a = 1.5$ is used. Notice that r represents a dimension in the cross-shore direction, while j gives the other dimension in the along shore direction. Once the seafloor displacements are derived from the GPS measurements, they are then interpolated onto a grid over the fault area, which is defined by the source model.

As seawater is almost incompressible, the vertical displacement of seafloor in each increment would result in a similar motion on the sea-surface because water particles over the fault area cannot flow away before being pushed up. In addition, the horizontal displacements of slope also contribute vertically to the sea-surface deformation (Tanioka and Satake 1996). The total sea-surface perturbation due to the vertical motion (the vertical acceleration of water particles) in each increment is

$$\Delta\eta \approx \Delta h = \Delta U + \Delta E \times h_x + \Delta N \times h_y, \quad (4)$$

where η is the sea-surface elevation from the mean sea level, h is the water depth, Δ represents a small increment, and h_x and h_y are the eastward and northward slopes of the subfault surface, respectively. The tsunami potential energy gained by the ocean in each increment is

$$\Delta PE = g \times \rho \times \frac{\Delta\eta^2}{2} \times \Delta x \times \Delta y, \quad (5)$$

where g is the gravity acceleration and ρ is the water density. The total accumulated potential energy is the integration of Eq. (5) over the whole faulting area and within the period of rupture time.

To determine the kinetic energy transferred from a moving slope, we need the displacement velocity of the seafloor. Since each increment of the displacements has been achieved within a time interval of Δt s, the three-dimensional motion (velocity) of a sub-fault can be obtained by $(\Delta E, \Delta N, \Delta U)/\Delta t$. The vertical acceleration of water particles does not contribute to the tsunami propagation; however, the resultant sea-surface perturbation would give the ocean potential energy, which has been accounted for in Eq. (5). The accelerated horizontal velocity of water particles in the vicinity of moving slopes can be written as:

$$\Delta u_b(z) = \begin{cases} \Delta E/\Delta t, & -h \leq z \leq -R_x = h - \min\{h, L|h_x|\} \\ 0, & \text{otherwise} \end{cases} \quad (6)$$

$$\Delta v_b(z) = \begin{cases} \Delta N/\Delta t, & -h \leq z \leq -R_y = h - \min\{h, L|h_y|\} \\ 0, & \text{otherwise} \end{cases} \quad (7)$$

Here, t is the rise-time of the subfault, z is the vertical coordinate, and L_H is the effective range of the horizontal motion (Song et al. 2008). The tsunami kinetic energy gained by the ocean in each second due to the horizontal motion is

$$\Delta KE = \rho \times \frac{1}{2} (\Delta u_b^2 + \Delta v_b^2) \times \Delta z \times \Delta x \times \Delta y \quad (8)$$

where Δz is the vertical grid size in the bottom layer. The total accumulated kinetic energy is the integration of Eq. (8) over the whole faulting area and within

the period of rupture time. The sum of integrating Eqs. (5) and (8) gives the total tsunami source energy (E_T):

$$E_T = \sum_{i,j} \Delta PE + \sum_{i,j,k} \Delta KE \quad (9)$$

where the i , j , and k indicate the horizontal and vertical grid, respectively.

Appendix 2: DART Method

The National Oceanic and Atmospheric Administration (NOAA) has developed a tsunami forecast system assimilating real-time tsunami measurements from Deep-ocean Assessment and Reporting of Tsunami (DART) stations (<http://www.ndbc.noaa.gov/dart.shtml/>) for more accurate tsunami warnings (Titov et al. 2005; Titov 2009; Bernard and Titov 2015). The forecast system integrates three key components, the DART data, the pre-computed tsunami propagation database, and high-resolution, site-specific flooding forecast models. They correspond to the three distinct stages of tsunami evaluation: generation, propagation and coastal run-up. Together, these components provide a full forecast capability. Presently, the DART network is composed of 63 stations, and is globally owned by nine countries (Fig. 1b). The propagation database has 1990 unit scenarios covering the most active subduction zones in the Pacific, Indian and Atlantic Oceans. High-resolution flooding forecast models have been developed for 75 US coastal communities (54 in the Pacific, 21 in the Atlantic/Caribbean).

The tsunami forecast system has been tested with 40 past tsunamis and has shown good accuracy when compared with observed tsunami amplitude time series at tide gauges, particularly for destructive tsunami waves (Titov et al. 2005; Titov 2009; Wei et al. 2008, 2012; Tang et al. 2008, 2009, 2012, 2015; Bernard et al. 2014). The NOAA system is designed to predict tsunami flooding, but not all tsunamis produce flooding. However, during the 2011 Japanese tsunami the NOAA forecast system correctly predicted flooding at Kahalui, Hawaii 4 h before the tsunami arrived. Another feature of the NOAA

Center for Tsunami Research (NCTR) forecast system is to quickly estimate the tsunami energy. The total energy transmitted by tsunami waves is one of the most fundamental macroscopic quantities for quickly estimating the potential impact of a tsunami. As shown in Fig. 1b, DART stations are strategically positioned close to subduction zones throughout the world's oceans, where they detect tsunamis within 1 h of most tsunamis generated. In 2012, Japan installed three additional DART stations (Fig. 1) close to the Japanese coastline. With these additional stations, the December 7, 2012 Japanese tsunami energy could have been estimated within 20 min after the earthquake origin time (Bernard et al. 2014).

The DART inversion approach exploits the simple linearity assumption of tsunami propagation to circumvent the large uncertainties in earthquake sources. Wave dynamics of tsunami propagation in deep-ocean are assumed to be linear (Mei et al. 2005; Kanoglu and Synolakis 2006; Liu 2009). Therefore, a propagation scenario (η) can be decomposed into a superposition of a subset of source units (h):

$$h = \sum_{i=1}^N \alpha_i h_i \quad (10)$$

h is the tsunami amplitude, h_i is the tsunami amplitude of the i -th source unit, α_i is the i -th coefficient, N is the total number of source units used. A source unit h_i is a unit propagation scenario that could be generated by an earthquake, a landslide or other type of sources. Currently, each source unit h_i in the forecast system represents a unit propagation scenario generated by a typical Mw 7.5 subduction earthquake. It is modeled as the instantaneous rupture of a single rectangular fault plane characterized by pre-defined parameters described the location, orientation and rupture of the plane (Gusiakov 1978; Okada 1985). Each source unit has predefined parameters of length 100 km, width 50 km, slip 1 m and rake angle 90°. Other parameters, including depth, dip angle, and strike angle, are location-specific (Titov et al. 1999; Gica et al. 2008).

The DART-inverted tsunami source refers to the source scenario or the synthetic propagation scenario (η) from a superposition of source units (h) that gives a best fit to the observed tsunami amplitude time series (η_{obs}) in deep ocean:

$$\eta_{\text{obs}} = \eta + \text{res}_t = \sum_{i=1}^N \alpha_i h_i + \text{res}_t \quad (11)$$

$$\sum \text{res}_t^2 = \sum (\eta_{\text{obs}} - \eta)^2 = \sum \left(\eta_{\text{obs}} - \sum_{i=1}^N \alpha_i h_i \right)^2 \quad (12)$$

η_{obs} is the observed tsunami amplitude in deep ocean, res_t is a residual term between the observation and model. α_i was estimated using the least squares method (Eq. 12), e.g., minimizing the sum of the squared residuals (Percival et al. 2011).

The Method Of Splitting Tsunami (MOST) model, a suite of finite difference numerical codes based on the long-wave approximations (Titov and Synolakis 1998; Titov and Gonzalez 1997; Synolakis et al. 2008), is used to compute the tsunami propagation caused by source units:

$$\frac{\partial h}{\partial t} + \frac{\partial}{\partial x} [(h+d)u] + \frac{\partial}{\partial y} [(h+d)v] = 0 \quad (13)$$

$$\frac{\partial u}{\partial t} + u \frac{\partial u}{\partial x} + v \frac{\partial u}{\partial y} = -g \frac{\partial h}{\partial x} - \frac{C_f u |u|}{h+d} \quad (14)$$

$$\frac{\partial v}{\partial t} + u \frac{\partial v}{\partial x} + v \frac{\partial v}{\partial y} = -g \frac{\partial h}{\partial y} - \frac{C_f v |u|}{h+d} \quad (15)$$

where d is the undisturbed water depth, $u = \{u, v\}$, u and v are the depth-averaged velocities in the x and y directions, respectively, g is the gravity acceleration, f is the Coriolis parameter, $C_f = gn^2/(h+d)^{1/3}$, and n is Manning coefficient (assumed to be small during deep-ocean propagation). In the MOST model, these equations are solved numerically using the splitting method (Titov and Synolakis 1998).

At a given time, the instantaneous tsunami wave energy E is the sum of the kinematic energy, KE, and the potential energy PE. It is computed as:

$$E = \text{KE} + \text{PE} \quad (16)$$

where

$$\text{KE} = 0.5\rho \int_s (\eta+d)(u^2+v^2) ds$$

$$\text{PE} = 0.5\rho g \int_s \eta^2 ds$$

ρ is the ocean water density and g is the gravity acceleration coefficient. The integration is over the propagation domain S .

Based on the zero initial velocities assumptions according to the adopted elastic deformation model, the tsunami energy, E_T (the total energy transmitted by the tsunami waves), is then computed as the difference between the potential energy from the initial deformed body of water and that of the quiescent state in the same basin:

$$E_T = KE_{t=0} + PE_{t=0} = 0 + 0.5\rho g \int_S \eta_0^2 ds \quad (17)$$

where η_0 is the sea-surface elevation at the initial stage (e.g., the initial ocean surface deformation). Substituting Eq. (10) into Eq. (17), we have the numerical formula:

$$E_T = 0.5\rho g \sum_j s_j \left(\sum_{i=1}^N \alpha_i h_{0,i,j} \right)^2 \quad (18)$$

where j represents j -th wet grid node, s_j is a cell area corresponding to the j -th node, $h_{0,i,j}$ is the initial sea-surface displacement from the i -th tsunami source function at j -th node. More discussion on tsunami energy can be found in Tang et al. (2012).

REFERENCES

- Ambraseys, N. N. (1962). Data for the investigation of seismic sea waves in the Eastern Mediterranean. *Bulletin of the Seismological Society of America* 52, 895–913.
- Ando, M., Ishida, M., Hayashi, Y., & Mizuki, C. (2011). Interviews with survivors of Tohoku earthquake provide insights into fatality rate. *EOS Transitions AGU*, 92(48), 411–412.
- Bernard, E. N., & Titov, V. V. (2015). Evolution of tsunami warning systems and products. *Philosophical Transactions of the Royal Society*. doi:10.1098/rsta.2014.0371.
- Bernard, E. N., Wei, Y., Tang, L., & Titov, V. V. (2014). Impact of near-field, deep-ocean tsunami observations on forecasting the 7 December 2012 Japanese Tsunami. *Pure and Applied Geophysics*, 171 (12), 3483–3491. doi:10.1007/s00024-013-0720-8.
- Blewitt, G., Kreemer, C., Hammond, W. C., Plag, H.-P., Stein, S., & Okal, E. (2006). Rapid determination of earthquake magnitude using GPS for tsunami warning systems. *Geophysical Research Letters* 33, L11309. doi:10.1029/2006GL026145.
- Deguedre, H., Metzger, J. J., Geisel, T., & Fleischmann, R. (2016). Random focusing of tsunami waves. *Nature Physics*, 12, 259–262. doi:10.1038/nphys3557.
- Gica, E., Spillane, M. C., Titov, V. V., Chamberlin, C. D., & Newman, J. C. (2008). *Development of the forecast propagation database for NOAA's Short-term Inundation Forecast for Tsunamis (SIFT)*. NOAA technical memorandum OAR PMEL-139, NTIS: PB2008-109391. Seattle:NOAA/Pacific Marine Environmental Laboratory.
- Gusiakov, V. K. (1978). *Static displacement on the surface of an elastic space, in Ill-Posed Problems of Mathematical Physics and Interpretation of Geophysical Data (in Russian)* (pp. 23–51). Novosibirsk: Comput. Cent. of Sov. Acad. of Sci.
- Gusman, A. R., Tanioka, Y., Sakai, S., & Tsushima, H. (2012). Source model of the great 2011 Tohoku earthquake estimated from tsunami waveforms and crustal deformation data. *Earth and Planetary Science Letters*, 341, 234–242.
- Hammack, J. L., & Segur, H. (1974). The Korteweg-de Vries equation and water waves. Part 2. Comparison with experiments. *Journal of Fluid Mechanics*, 65(Part 2), 289–314.
- Iida, K. (1956). Earthquakes accompanied by tsunamis occurring under the sea off the islands of Japan. *Journal of Earth Sciences, Nagoya University*, 4, 1–43.
- Imamura, A. (1942). History of Japanese tsunamis. *Kayo-No-Kagaku (Oceanography)*, 2, 74–80. (in Japanese).
- Ito, Y., et al. (2011). Frontal wedge deformation near the source region of the 2011 TohokuOki earthquake. *Geophysical Research Letters*, 38, L00G05.
- Jouhana, D., & Paddock R. C. (2006). Indonesia quake kills 3500, *Chicago Tribune*. http://articles.chicagotribune.com/2006-05-28/news/0605280253_1_bantul-quake-caused-widespread-panic-rush-tents.
- Kanoglu, U., Titov, V., Bernard, E., & Synolakis, C. (2015). Tsunami: bridge the science, engineering and social science. *Philosophical Transactions of the Royal Society A*, 373(2053), 20140369.
- Kanoglu, U., & Synolakis, C. E. (2006). Initial value problem solution of nonlinear shallow water wave equations. *Physical Review Letters*, 97(14), 148501. doi:10.1103/PhysRevLett.97.148501.
- Liu, P. L. F. (2009). Tsunami modeling: Propagation. In E. Bernard, et al. (Eds.), *The Sea, Tsunamis Ch. 3* (15th ed., pp. 295–320). Cambridge: Harvard University Press.
- Mei, C. C., Tiassnie, M., & Yue, D. (2005). *Theory and applications of ocean surface waves, part 1: Linear aspects*. Singapore: World Scientific.
- Morgan, R. (2011). Top 100 stories of 2010, #84: Yardstick for killer waves, Discover. <http://discovermagazine.com/2011/jan-feb/84/>.
- Murty, T. S., & Loomis, H. G. (1980). A new objective tsunami magnitudes scale. *Marine Geodesy*, 4, 267–282.
- Naranjo, L. (2013). Sizing a tsunami, sensing out planet. *NASA Science Research Features 2013*, pp. 30–33. <https://earthdata.nasa.gov/featured-stories/featured-research/sizing-tsunami/>.
- NASA release (2010). http://www.nasa.gov/topics/earth/features/tsunami_prediction.html.
- Okada, Y. (1985). Surface deformation due to shear and tensile faults in a half space. *Bulletin of the Seismological Society of America*, 75, 1135–1154.
- Okal, E. A. (2015). The quest for wisdom: Lessons from 17 tsunamis, 2004–2014. *Philosophical Transactions of the Royal Society A*, 373, 20140370. doi:10.1098/rsta.2014.0370.
- Okal, E. A., & Synolakis, C. E. (2016). Sequencing of tsunami waves: Why the first wave is not always the largest. *Geophysical Journal International*, 204(2), 719–735.
- Papadopoulos, G. A., & Imamura, F. (2001). *A proposal for a new tsunami intensity scale Internat. Tsunami symposium 2001 Proc.*, Seattle, Washington, Aug. 7–10, 2001, pp. 569–577.

- Percival, D. B., Denbo, D. W., Eble, M. C., Gica, E., Mofjeld, H. O., Spillane, M. C., et al. (2011). Extraction of tsunami source coefficients via inversion of DART® buoy data. *Natural Hazards*, 58(1), 567–590. doi:10.1007/s11069-010-9688-1.
- Satake, K., Nishimura, Y., Putra, P. S., Gusman, A. R., Sunendar, H., Fujii, Y., & Yulianto, E. (2013). Tsunami source of the 2010 Mentawai, Indonesia earthquake inferred from tsunami field survey and waveform modeling. *Pure and Applied Geophysics*, 170(9–10), 1567–1582.
- Sieberg, A. (1927). *Geologische, physikalische and angewandte Erdbebenkunde*. Jena: Verlag von Gustav Fischer.
- Song, Y. T., Ji, C., Fu, L.-L., Zlotnicki, V., Shum, C. K., Yi, Y., & Hjorleifsdottir, V. (2005). The 26 December 2004 Tsunami source estimated from satellite radar altimetry and seismic waves. *Geophysical Research Letters*,. doi:10.1029/2005GL023683.
- Song, Y. T. (2007). Detecting tsunami genesis and scales directly from coastal GPS stations. *Geophysical Research Letters*, 34, L19602. doi:10.1029/2007GL031681.
- Song, Y. T., Fu, L.-L., Zlotnicki, V., Ji, C., Hjorleifsdottir, V., Shum, C. K., & Yi, Y. (2008). The role of horizontal impulses of the faulting continental slope in generating the 26 December 2004 Tsunami. *Ocean Modelling*,. doi:10.1016/j.ocemod.2007.10.007.
- Song, Y. T., & Han, S. C. (2011). Satellite observations defying the long-held tsunami genesis theory. In D. L. Tang (Ed.), *Remote sensing of the changing oceans*. Berlin: Springer. doi:10.1007/978-3-642-16541-2.
- Song, Y. T., Fukumori, I., Shum, C. K., & Yi, Y. (2012). Merging tsunamis of the 2011 Tohoku-Oki earthquake detected over the open ocean. *Geophysical Research Letters*, 39, L05606. doi:10.1029/2011GL050767.
- Stein, S., & Okal, E. A. (2005). Speed and size of the Sumatra earthquake. *Nature*, 434(7033), 581–582.
- Synolakis, C., Bernard, E., Titov, V., Kanoglu, U., & Gonzalez, F. (2008). Validation and verification of tsunami numerical models. *Pure and Applied Geophysics*, 165(11–12), 2197–2228. doi:10.1007/s00024-004-0427-y.
- Tang, L., Titov, V. V., & Chamberlin, C. D. (2009). Development, testing, and applications of site-specific tsunami inundation models for real-time forecasting. *Journal of Geophysical Research*, 114, C12025. doi:10.1029/2009JC005476.
- Tang, L., Titov, V. V., Wei, Y., Mofjeld, H. O., Spillane, M., Arcas, D., et al. (2008). Tsunami forecast analysis for the May 2006 Tonga tsunami. *Journal of Geophysical Research*, 113, C12015. doi:10.1029/2008JC004922.
- Tang, L., Titov, V. V., Bernard, E. N., Wei, Y., Chamberlin, C. D., Newman, J. C., et al. (2012). Direct energy estimation of the 2011 Japan tsunami using deep-ocean pressure measurements. *Journal of Geophysical Research*, 117, C08008. doi:10.1029/2011JC007635.
- Tang, L., Titov, V. V., Moore, C., & Wei, Y. (2015). Real-time assessment of the 16 September 2015 Chile Tsunami and implications for near-field forecast. *Pure and Applied Geophysics*. (in review).
- Tanioka, Y., & Satake, K. (1996). Tsunami generation by horizontal displacement of ocean bottom. *Geophysical Research Letters*, 23(8), 861–864.
- Titov, V. V., & Synolakis, C. E. (1995). Modeling of Breaking and Nonbreaking Long Wave Evolution and Runup using VTCS-2. *Journal of Waterways, Ports, Coastal and Ocean Engineering*, 121(6), 308–316.
- Titov, V. V., & Synolakis, C. E. (1998). Numerical modeling of tidal wave runup. *Journal of Waterway, Port, Coastal and Ocean Engineering*, 124(4), 157–171.
- Titov, V. V., & Gonzalez, F. I. (1997). *Implementation and testing of the Method of Splitting Tsunami (MOST) model*. NOAA Tech. Memo. ERL PMEL-112. Seattle: Pacific Marine Environmental Laboratory.
- Titov, V. V., Mofjeld, H. O., Gonzalez, F. I., & Newman, J. C. (1999). *Offshore forecasting of Alaska-Aleutian subduction zone tsunamis in Hawaii*. Tech. Memo. ERL PMEL-114 (p. 22). Seattle: Gov. Print. Off..
- Titov, V. V., González, F. I., Bernard, E. N., Eble, M. C., Mofjeld, H. O., Newman, J. C., & Venturato, A. J. (2005). Real-time tsunami forecasting: Challenges and solutions. *Natural Hazards*, 35(1), 41–58.
- Titov, V. V. (2009). Tsunami forecasting. In E. N. Bernard (Ed.), *The Sea, Tsunamis Ch. 12* (15th ed.). Cambridge: Harvard Univ. Press.
- Titov, V. V., Moore, C. W., Greenslade, D. J. M., Pattiaratchi, C., Badal, R., Synolakis, C. E., & Kanoglu, U. (2011). A new tool for inundation modeling: Community Modeling Interface for Tsunamis (ComMIT). *Pure and Applied Geophysics*, 168, 2121–2131. doi:10.1007/s00024-011-0292-4.
- Wei, Y., Bernard, E. N., Tang, L., Weiss, R., Titov, V. V., Moore, C., et al. (2008). Real-time experimental forecast of the Peruvian tsunami of August 2007 for US coastlines. *Geophysical Research Letters*, 35, L04609. doi:10.1029/2007GL032250.
- Wei, Y., Chamberlin, C., Titov, V. V., Tang, L., & Bernard, E. N. (2012). Modeling of 2011 Japan Tsunami: Lessons for near-field forecast. *Pure and Applied Geophysics*. doi:10.1007/s00024012z.
- Wei, Y., Chamberlin, C., Titov, V., Tang, L., & Bernard, E. N. (2013). Modeling of the 2011 Japan tsunami—lessons for near-field forecast. *Pure and Applied Geophysics*, 170(6–8), 1309–1331. doi:10.1007/s00024-012-0519-z.
- Wei, Y., Newman, A. V., Hayes, G. P., Titov, V. V., & Tang, L. (2014). Tsunami forecast by joint inversion of real-time tsunami waveforms and seismic or GPS data: Application to the Tohoku 2011 tsunami. *Pure and Applied Geophysics*, 171(12), 3281–3305. doi:10.1007/s00024-014-0777-z.
- Xu, Z., & Song, Y. T. (2013). Combining the all-source Green's functions and the GPS-derived source for fast tsunami prediction—illustrated by the March 2011 Japan tsunami. *Journal of Atmospheric and Oceanic Technology*. doi:10.1175/JTECH-D-12-00201.1.